JPhys Materials

PURPOSE-LED PUBLISHING™

ACCEPTED MANUSCRIPT • OPEN ACCESS

Bi_2WO_6 thin films grown by high-power InfraRed Nd:YAG Pulsed Laser Deposition: a structural and spectroscopic study

To cite this article before publication: Lorenzo Arici *et al* 2025 *J. Phys. Mater.* in press https://doi.org/10.1088/2515-7639/adb51b

Bi_2WO_6 thin films grown by high-power InfraRed Nd:YAG Pulsed Laser Deposition: a structural and spectroscopic study

Lorenzo Arici[a,b], Carolina Gutierrez Bolanos[c], Sandeep Kumar Chaluvadi[d], Shyni Punathum Chalil[d,e], Ivana Vobornik[d], Jun Fujii[d], Federico Mazzola[f], Maria Eugenia Fortes Brollo[c], Regina Ciancio[g], Andrea Goldoni[c], Pasquale Orgiani[d,‡] and Marco Caputo[c,h]

[a] *University of Trieste, 34127 Trieste, Italy*
[b] *Weizmann Institute of Science, 7639302 Rehovot, Israel*
[c] *Elettra Sincrotrone Trieste S.C.p.A., 34149 Trieste, Italy*
[d] *CNR-IOM Istituto Officina dei Materiali, 34149 Trieste, Italy*
[e] *International Centre for Theoretical Physics (ICTP), 34151 Trieste, Italy*
[f] *CNR-SPIN Istituto superconduttori, materiali innovativi e dispositivi, 80125 Napoli, Italy*
[g] *AREA Science Park, 34149 Trieste, Italy*
[h] *MAX IV Laboratory, Lund Uiversity, 22484 Lund, Sweden*
[‡] *Corresponding author: pasquale.orgiani@cnr.it*

Abstract. We report on the epitaxial growth of Bi_2WO_6 thin films by Pulsed Laser Deposition using a high-power infrared Nd:YAG laser source. X-ray diffraction investigation confirms that single (00*l*)-oriented thin films can be obtained on both LSAT and $SrTiO_3$ substrates by using a $LaNiO_3$ adapting layer. Moreover, reciprocal space maps show that the films coherently grow on such substrates with the in-plane lattice parameters fully matching those of the substrates. In-situ x-ray photoemission spectroscopy experiments show that a UHV annealing process makes the film more conductive even though it also affects the Bi:W chemical ratio by reducing the Bi content. Alternately, the conductivity of the films can be effectively tuned by either growing the film in Ar atmosphere or by depositing potassium on its surface without modifying the Bi:W chemical ratio. Our results provide a viable route to synthesize high-quality Bi_2WO_6 thin films with tailored electronic properties.

1. Introduction

Bismuth tungstate Bi_2WO_6 (BWO) is a compound within the Aurivillius family of layered perovskite materials and crystallizes in an orthorhombic structure characterized by alternating layers of Bi_2O_2 units and WO_4 octahedra (Fig. 1) [1]. Its layered architecture endows the material with distinct anisotropic properties and a high degree of chemical stability which has garnered significant attention in recent years due to its unique structural, optical, and electronic properties [2]. For instance, BWO has been considered a promising candidate in the field of photocatalysis for degrading organic pollutants and generating hydrogen through water splitting [3–7] and its non-toxic and environmentally benign nature enhances its attractiveness for sustainable applications. In addition, BWO has also been explored for electro-optical applications, including ferroelastic [8], ferroelectric [9, 10], and dielectric materials and sensors

[11–13]. In particular, its ferroelectric properties, derived from the distortion of the WO_4 octahedra [12, 14], offer opportunities for use in non-volatile memory devices and other electronic components [11]. Besides being a ferroelectric with a sizable Rashba splitting, its layered structure creates a unidirectional spin-orbit field protecting the spin transport from spin dephasing [12]. Overall, BWO represents a versatile material with a wide array of functional applications, driven by its unique structural characteristics and favorable electronic properties. Controlling its structure is expected to allow for control of its electronic properties [15–18] thus pushing the research activity in the field of synthesis of BWO [2, 13, 19, 20].

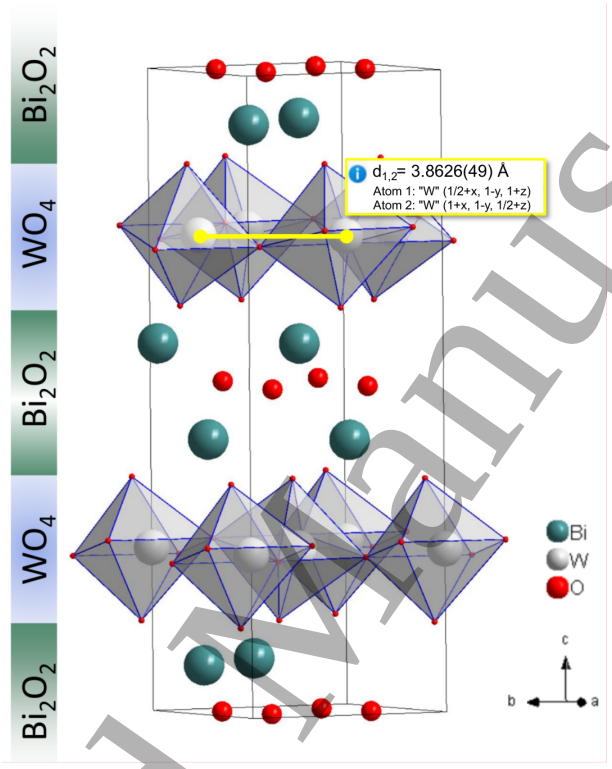

Figure 1. Sketch of BWO unit cell along the [001] crystallographic direction showing the stacking of Bi_2O_2 blocks and WO_4 octahedra.

Here, we present results on synthesizing BWO thin films that epitaxially grow with a single-phase orientation. An annealing process at high temperatures and in UHV conditions can increase the BWO films' overall conductivity by removing oxygen from the films, but it also affects the Bi:W optimal stoichiometry. Comparable electron doping can be obtained in as-grown films synthesized in an Ar environment without any post-annealing process. While the growth in Ar dopes BWO in its bulk, the electronic properties at its surface can only be modulated by evaporating potassium on the films. However, in all these cases, the BWO insulating state appears robust to n-doping as we never observed its conduction band crossing the Fermi energy. Our results provide viable routes to synthesize high-quality BWO thin films and craft their physical properties precisely.

2. Structural and chemical characterization of thin films

BWO thin films were grown using an Nd:YAG laser operating at its fundamental wavelength (i.e. 1064 nm) which falls in the infra-red region. Such a laser source has a pristine spot size of the laser shot of about 0.6 cm in diameter with a typical energy of 700 mJ, corresponding to an energy density U of about 2.5 J/cm^2 for the unfocused beam, which was verified to already ablate target. Nonetheless, the laser beam was focused on the target, with U reaching the estimated value above 20 J/cm^2 making such a deposition condition uncommon when compared to PLD-processes realized by the use of KrF excimer lasers in which energy U typically ranges between $1 \div 5$ J/cm^2. Moreover, while the typical duration of the excimer laser shot is about 25 ns, Nd:YAG lasers provide such an intense laser shot with a typical duration of $6 \div 10$ ns. Relevant information of both Nd:YAG and KrF laser sources are reported in Table.1 Although operating in quite different conditions in terms of energy, duration, and wavelength, high-power infrared Nd:YAG lasers have been capable of successfully growing a large variety of samples [14, 21, 22]. Moreover, differently from the PLD-process assisted by an excimer laser, Nd:YAG laser at fundamental harmonics efficiently ablates also metal disks (e.g. Co, Fe, Dy), thus further increasing the number of materials that can be deposited as multilayered structures within a single deposition run.

Table 1. Key-parameters of Nd:YAG and KrF lasers

Laser Parameters	Nd:YAG laser	KrF laser
Wavelength	1064 nm	248 nm
Fluence of a single laser shot	700 mJ	$200 \div 340$ mJ
Energy density of unfocused beam	~ 2.5 J/cm^2	~ 0.1 J/cm^2
Energy density of focused beam	~ 20 J/cm^2	$2 \div 3$ J/cm^2
Pulse width	$6 \div 10$ ns	~ 25 ns

The lattice parameters of $Pca2_1$ orthorhombic phase of bulk BWO are as follows: a = 0.54345(12) nm, b = 0.54558(12) nm and c = 1.64324(12) nm [23, 24]. Along the (110)-crystallographic direction, a nearly-square arrangement with in-plane lattice parameters of $a_p = 0.3838$ nm and $b_p = 0.3863$ nm can be resolved (see Fig.1). Therefore, epitaxial growth of BWO is expected on substrates that are usually used for the growth of oxides [25]. BWO films were grown using pulsed laser deposition (PLD) [26] with a solid-state Nd:YAG infrared laser source [21] on $(LaAlO_3)_{0.3}(Sr_2TaAlO_6)_{0.7}$ (LSAT) and 1%at Nb-doped $SrTiO_3$ (STO) substrates where a small lattice mismatch is expected, namely -0.5% and -1.4% on LSAT and STO, respectively. To improve the BWO crystallographic quality, a deposition of a $LaNiO_3$ (LNO) buffer layer was routinely done. As a matter of fact, the insertion of an LNO as an adapting layer has been previously proven to inhibit the interdiffusion of heavy cations from the substrates and the occurrence of spurious phase at film/substrate interface [27]. Indeed, BWO films directly grown on substrates do not show any crystallographic order thus indicating either the polycrystalline or the amorphous nature of the grown films as probed by X-ray diffraction

(XRD). On the other hand, the insertion of an LNO buffer layer largely improves the films' crystallinity, resulting in them all being well-aligned along a single crystallographic direction (Fig.S1 in supplementary).

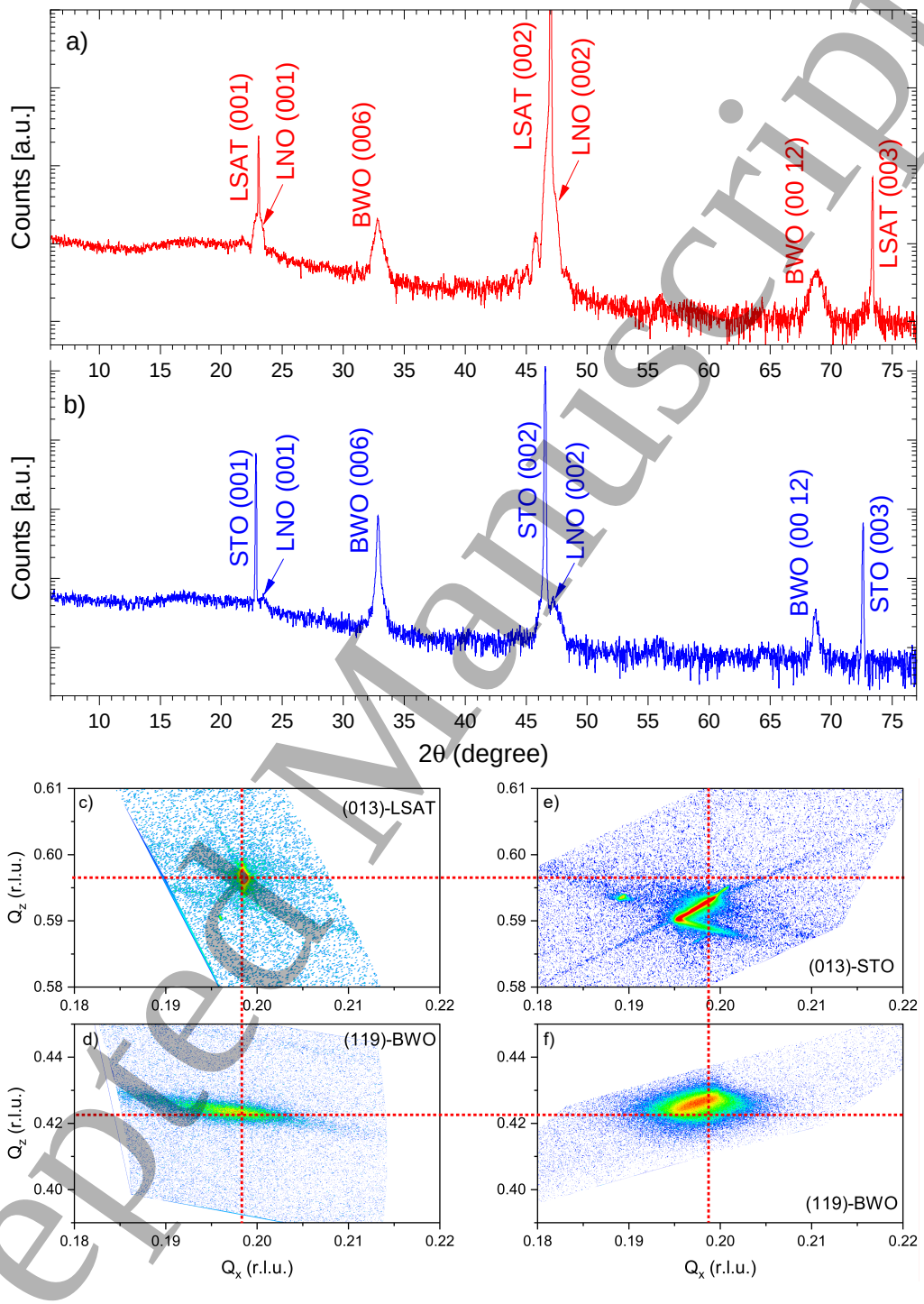

Figure 2. (a-b) Symmetrical θ - 2θ scans of BWO films grown on LSAT (red) and Nb:STO (blue) substrates, respectively; reciprocal space maps around (119)-BWO and (013)-LSAT (c-d) and Nb:STO (e-f) substrates reflections (the position of BWO-on-LSAT diffraction peaks are reported as red crosses in both panels).

Symmetrical θ - 2θ scans of optimized BWO films grown on LSAT and STO substrates

with a 10 nm-thick LNO buffer layer are reported in panels a) and b) in Fig. 2. In both cases, XRD spectra only contain (00*l*) peaks thus indicating the preferential c-axis orientation of the film along the [001] crystallographic direction of substrates. By the position of the symmetric (006) Bragg reflections, the out-of-plane c-axis parameters were calculated to be 1.640 nm and 1.637 nm for films grown on LSAT and STO substrates, respectively. When compared with the value of 1.643 nm reported for single crystals [23, 24], the obtained values indicate a shrinking of the BWO unit cell, as expected by a coherent tensile strained growth on those substrates. To investigate the substrate/film structural in-plane relationship, reciprocal space maps of BWO around suitable asymmetric reflections were performed.

As a matter of fact, for asymmetric reflections, the scattering vectors have components both in and out of the plane of the sample and these are visible at specific azimuthal angles because the alignment of the lattice planes and the sample's rotational orientation [28]. In particular, Fig 2d and Fig. 2f show the BWO (119) diffraction peaks along with (013) LSAT (Fig. 2c) and (013) STO (Fig. 2e) diffraction peaks, respectively. Since symmetrical θ-2θ scans have demonstrated the [00*l*]-orientation for both BWO films and LSAT/STO substrates, the (013)-substrate is given by [010]+[003] reciprocal vectors while the (119)-BWO is given by [110]+[009] reciprocal vectors. In the reported reciprocal space maps, being those peaks detected at the same $\phi = 0^\circ$ angle, the BWO[110]//substrate[010] parallelism relation can be derived. A further proof of the in-plane crystallographic relationship is provided by the reciprocal space map around (113)-LSAT and (01 10)-BWO recorders at $\phi = 45^\circ$ angle (Fig.S2 in supplementary) which sets the BWO[010]//LSAT[110] parallelism relationship. In other words, considering the [010]-crystallographic orientation for both the BWO film and LSAT/STO substrates, they have been observed at 45° apart for the azimuthal angle thus confirming that BWO grows in-plane 45°-rotated with respect to the in-plane crystallographic axes of substrates. Moreover, in both cases, substrate and film diffraction peaks are well aligned along the Q_x directions, thus inferring that BWO grows fully strained with both substrates. Moreover, the increase of the in-plane lattice parameter for the BWO films grown on STO (i.e. smaller value of Q_x) corresponds to a shirking of its out-of-plane lattice parameter (i.e. larger value of $Q_{z)}$), in full agreement with data obtained by the analysis of symmetric reflections thus confirming the coherent elastic deformation of BWO.

The surface roughness of both LNO and BWO-on-LNO films was probed by low-angle X-ray reflectivity (XRR) and reported in Fig. 3. Numerical simulations of the low-angle XRR data (i.e., line-curves in panels a and b of Fig. 3) were performed using the AMASS software by Malvern. For the LNO buffer layer, the XRR curve oscillates up to 2θ values of about 5.5°, therefore setting a value for the surface roughness to about 0.4 nm, corresponding to an LNO single unit cell. On the contrary, the surface roughness of BWO thin films is higher than the LNO buffer layer being XRR oscillations damped for 2θ values above 2.5°. Yet, also in this case, the estimated RMS value of about 1.6 nm is very close to a BWO single unit cell (i.e. about 1.64 nm).

Surface long-range order was probed by in-situ Low-Energy Electron Diffraction (LEED) technique. The use of low-energy electrons in the LEED technique sets a series of requirements on the nature of the material under investigation. In particular, insulating materials tend

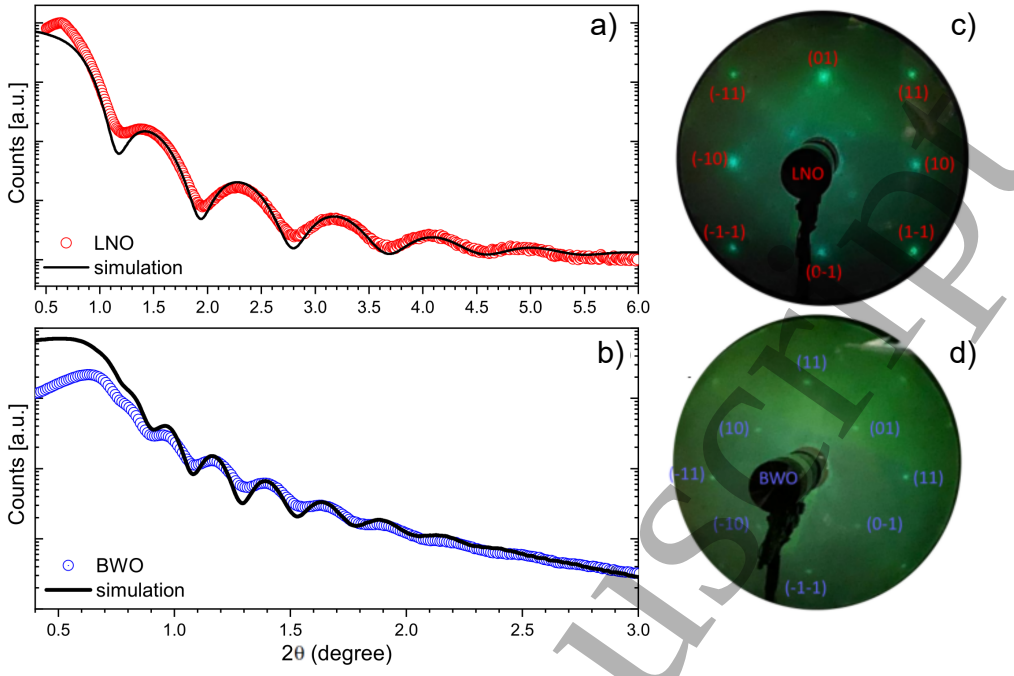

Figure 3. X-ray reflectivity of 10-nm-thick LNO (a; red dots) and 33-nm-thick BWO (b; blue dots) films grown on STO substrates and the correspondent fitting curves (continuous lines) with selected values of RMS; LEED patterns of an LNO film (c) and a BWO film grown on LNO-buffered substrates (d).

to accumulate surface charges when electrons are incident on them thus distorting the diffraction pattern of diffracted electrons. As-grown BWO films showed no LEED pattern most likely because of their non-conductive nature. However, as demonstrated for other oxides [29–33], a post-annealing process in UHV-condition is expected to promote oxygen vacancies into the films and, as a consequence, make them more conductive. An annealing was therefore performed on as-grown samples soon after the deposition, at higher temperatures and residual vacuum conditions (i.e. below 10^{-6} mbar). After such a process, a LEED pattern, measured by electrons with ∼60 eV kinetic energy was observed. The lack of any trace of a continuous connecting ring between the spots indicates the absence of a randomly in-plane distributed disordered phase. Moreover, surface contamination (e.g., droplets, see Fig.S3 in supplementary) that are known to disrupt the LEED pattern typically by broadening the spots or reducing the contrast of the diffraction spots, are ruled out by the presence of sharp diffraction spots (panel d in Fig. 3). The observed LEED pattern is compatible with a single domain exhibiting a four-fold symmetry and 45° rotated with respect to the square coordination of the (001)-oriented LNO buffer layer (panel c of Fig. 3), which is aligned with those of both LSAT/STO substrates.

3. Doping mechanisms investigated by x-ray photoemission spectroscopy

Although a UHV-annealing process at high temperatures was demonstrated to increase the conductivity of BWO films, questions arise about the real origin of this phenomenon. In par-

ticular, because of the well-known high volatility of bismuth [34], it is crucial to understand if the BWO structural/chemical stoichiometry was preserved after the thermal treatment. From the structural point of view, XRD θ - 2θ scans show the occurrence of the BWO phase only without any trace of spurious ones. However, differently to what occurs in many other perovskite oxide systems [35–37] where oxygen vacancies are known to expand the out-of-plane lattice parameter, here the diffraction peaks of the annealed samples shift to higher angles thus pointing to a shrinking of the BWO unit cell (Fig.S4 in supplementary). Such a result therefore questions the assumption that the final UHV-annealing process only promotes oxygen vacancies.

To shed light on this issue, the Bi:W stoichiometry ratio was therefore investigated using X-ray Photoemission Spectroscopy (XPS) [38]. Fig. 4a directly compares W_{4f} and Bi_{5d} peaks for both as-grown and UHV-annealed BWO samples. The Bi:W stoichiometry was quantitatively determined by a fitting procedure based on the Bi_{5d}/W_{4f} areas and the XPS cross-section. Due to possible errors in the fitting routine and background subtraction and the presence of the photoelectron diffraction effect, the experimental error in determining the chemical composition by XPS can be as large as 10%. The as-grown sample has a Bi:W ratio of about 1.9, which is compatible with the Bi_2WO_6 optimal stoichiometry. However, the annealed sample shows a Bi:W ratio of about 1.7, thus pointing to a Bi deficiency on the BWO films after UHV annealing process [34].

Since the UHV annealing process was shown to promote Bi off-stoichiometry, we adopted an alternative method to electron-dope oxide thin films via the growth in an Ar rather than O_2 atmosphere. In this way, while the inert behavior of argon should leave unchanged the impinging energy of the ablated species as well as their relative amount reaching the substrate [39–41], a significant reduction of oxygen content in the growing BWO films is expected. While it was not possible to perform XPS investigation on as-grown samples by using 45 eV impinging photons because of charging effects, BWO films grown in argon were sufficiently conducting to allow it, and a direct comparison with UHV-annealed BWO samples was therefore possible. As expected, the XPS spectrum of the sample grown in Ar atmosphere does not show deviation from the optimal Bi:W chemical composition (Fig. 4d) and a small shift to lower binding energies of the valence band (see procedure in Fig. 4b) with respect to the films grown in oxygen and subsequently post-annealed in UHV (Fig. 4c). It is therefore straightforward that, for samples grown in argon, the energy position of the valence band is triggered only by oxygen content in the films, rather than a heavy-ions off-stoichiometry. Moreover, such a result also paves the way for its fine-tuning by varying the oxygen/argon mixture in the deposition background environment.

While the growth in argon creates oxygen vacancies within the whole film, the strategy for electron-doping the BWO films only at its surface calls for the in-situ evaporation of alkali metals. Fig. 5a shows XPS spectra of a BWO sample with different potassium content on its surface. Potassium doping was performed by exposing the sample's surface held at a temperature of about 77 K to a potassium getter (SAES getter). The getter was heated at a current of 6.5 A and held at a distance of about 10 cm from the sample surface. The deposition time is intended as incremental from the unexposed surface condition (i.e., the first curve is after 1' of deposition, the second curve is after $1' + 5' = 6'$ minutes of deposition, and so on). As shown, the energy position of the Fermi energy (Fig. 5b) can be effectively varied by the

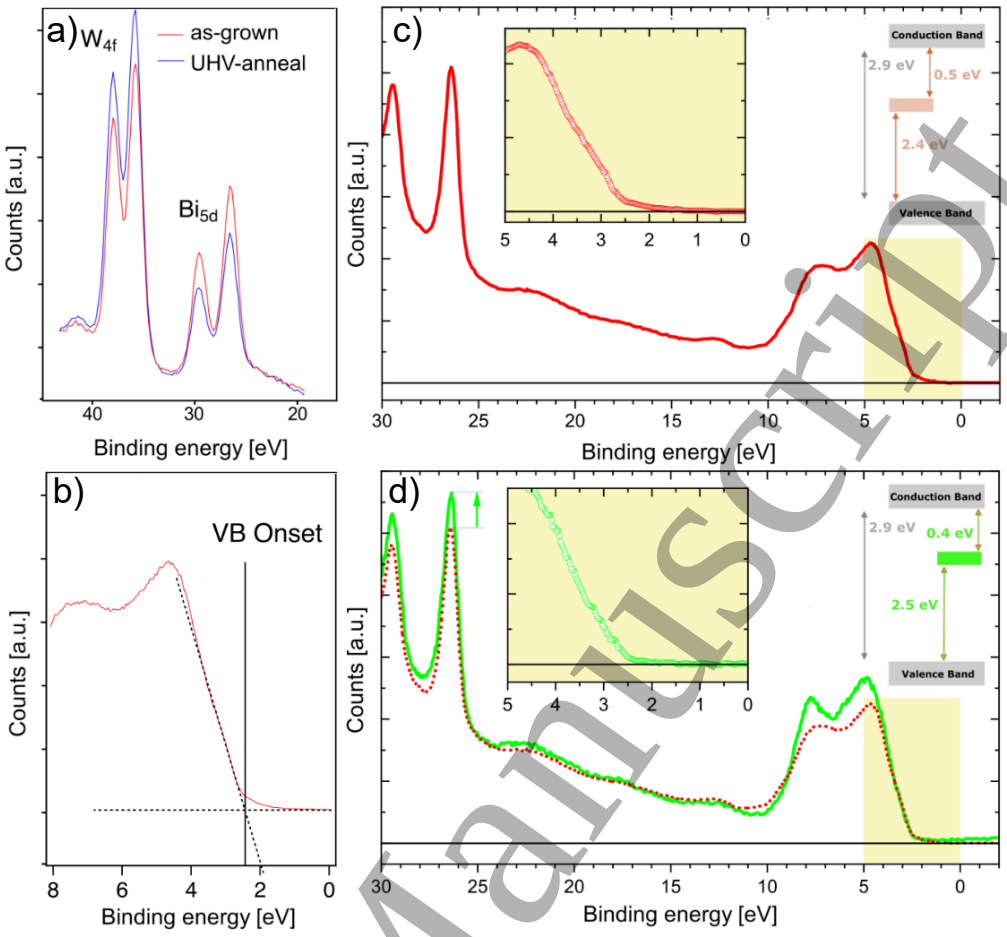

Figure 4. (a) XPS spectra around W_{4f} and Bi_{5d} of the annealed (blue) and the not annealed (red) ones; (b) visual sketch of the fitting procedure to extract the value of the valence band onset; XPS spectra of BWO samples grown in oxygen and subsequently annealed in UHV (c) and grown in Argon (d) atmosphere; in particular, the spectra in (c) is also reported as dotted lines in (d); the position of the Fermi energy is evaluated by assuming an energy gap of 2.9 eV.

potassium content up to 16 minutes of evaporation when undesired clusters were formed on the film surface as demonstrated by the different chemical environments of the Bi atoms correlated to a new Bi peak around 24 eV of binding energy marked by an asterisk in Fig. 5a.

Interestingly, all of the doping mechanisms here presented are effective in tuning the energy position of the valence band, although not capable of sufficiently populating the conduction band and turning the BWO into a full metal. Such a result shows the robustness of the insulating state in BWO compound.

4. Conclusions

The obtained results can be summarized as follows:

(i) Both LSAT and STO substrates allow the growth of single-oriented BWO epitaxial thin films; the small film/substrate in-plane mismatch allows a coherent growth of BWO which is found to be fully strained with both the substrates;

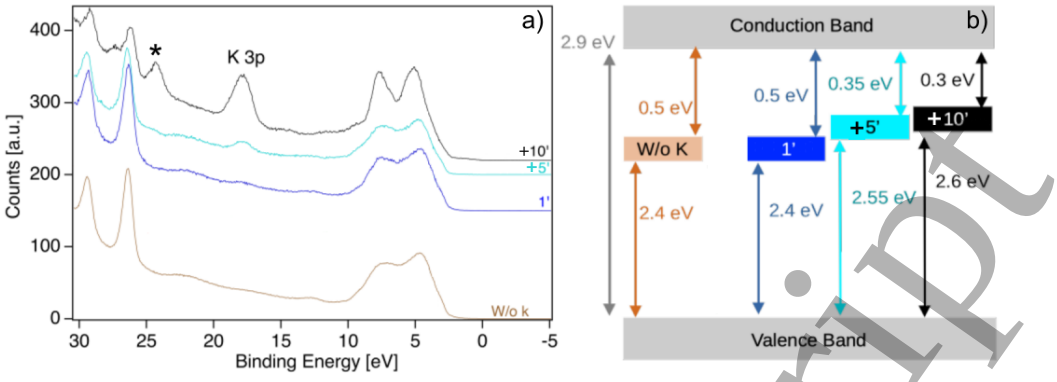

Figure 5. (a) Spectra of the BWO sample with a different amount of potassium on its surface and (b) the corresponding Fermi energy evaluated by assuming an energy gap of 2.9 eV.

(ii) a thin (i.e. 10 nm) LNO buffer layer improves the structural properties of grown BWO films allowing the single-phase orientation of the films without affecting the in-plane lattice coordination;

(iii) an annealing process in UHV condition is capable of increasing the metallicity of the BWO films, yet promoting Bi:W off-stoichiometries by sublimating Bi;

(iv) electron-doping is possible by growing BWO films in Ar atmosphere rather than in oxygen without affecting the Bi:W ratio;

(v) potassium evaporation on the BWO films is also able to fine-tune the position of the valence band, though not able to turn into full metal compounds (i.e. the conduction band crossing Fermi level).

Our results provide a viable route to synthesize high-quality Bi_2WO_6 thin films with ad-hoc tailored electronic properties. Unlike conventional PLD systems based on ultraviolet excimer lasers, the deposition process relies on a solid-state Nd:YAG pulsed laser source operating at its fundamental wavelength in the infrared region. Such lasers overcome a series of limitations arising when traditional KrF excimer lasers are used such as safety issues (e.g. presence of highly poisonous gases) and the overall cost of the installation (e.g. reduced cost of a Nd:YAG laser source with respect an excimer one, negligible maintenance compared to the expensive gas mixture necessary for the KrF). The higher flexibility of such a laser combined with the high quality of the obtained compounds pave the way for fabricating heterostructures of very high quality grown by PLD in an all-in-situ approach.

Material and methods

BWO films were grown using pulsed laser deposition (PLD) with a laser source of a solid-state Nd:YAG infra-red laser [21, 26]. The pristine spot size of 0.6 cm in diameter was reduced to 0.2 cm by using optical masks and subsequently focused on the target. Though a precise estimate of the spot size on the target position is not possible, an energy density value above 20 J / cm^2 was estimated. A Bi:W:O = 2:1:6 stoichiometric pressed-powders target was used. The frequency of the laser was set at 0.5 Hz. The growth rate for LNO and BWO layers was 0.01 nm/laser-shot and 0.03 nm/laser-shot, respectively. The deposition temperature was kept at

420°C and the O_2/Ar background pressure of 10^{-1} mbar. LNO buffer layer was deposited at the same deposition pressure and 670°C.

X-ray diffraction (XRD) characterization was carried out by a Malvern Empyrean 4-circles diffractometer equipped with a double-bounce 2xGe(220) hybrid monochromator providing the K_{α_1} (1.540598 Å) wavelength only. GaliPIX3D detector with a 481 x 465 pixels active window (corresponding to an equatorial and an axial sizes of 6.8898° and 5.7632°, respectively) was used.

Low-Energy Electron Diffraction (LEED) patterns were measured by electrons with ∼60 eV kinetic energy on untreated BWO samples soon after the growth and transferred in UHV condition (i.e. in the range of 10^{-9} mbar).

The electronic states at the surfaces of BWO samples were investigated by in-situ x-ray photoemission spectroscopy (XPS) with synchrotron radiation of 45 eV and a Scienta DA30 hemispherical electron analyzer [42]. The energy scale was calibrated using the Fermi level of gold with an overall energy resolution of about 50 meV.

Author Contributions

Marco Caputo: conceptualization, supervision; Pasquale Orgiani: writing – original draft; All of the authors: investigation, methodology, formal analysis, validation, data curation, writing – review & editing;

Conflicts of interest

There are no conflicts to declare.

Data availability

The data that support the findings of this study are available upon reasonable request from the corresponding author.

Acknowledgements

This work has been performed in the framework of the Nanoscience Foundry and Fine-Analysis (NFFA-MUR Italy Progetti Internazionali) facility.

References

[1] Frit B and Mercurio J 1992 *Journal of Alloys and Compounds* **188** 27–35 ISSN 0925-8388 URL https://doi.org/10.1016/0925-8388(92)90639-Q

[2] Liu X, Long P, Sun Z and Yi Z 2016 *Journal of Materials Chemistry C* **4** 7563–7570 ISSN 2050-7526 URL https://doi.org/10.1039/C6TC02069K

[3] Wu S, Sun J, Li Q, Hood Z D, Yang S, Su T, Peng R, Wu Z, Sun W, Kent P R C, Jiang B and Chisholm M F 2020 *ACS Applied Materials & Interfaces* **12** 20067–20074 ISSN 1944-8244 URL https://doi.org/10.1021/acsami.0c01802

[4] Peng D, Zou Z, Long F, He J and Zhang T 2016 *Ionics* **22** 2347–2353 ISSN 0947-7047 URL https://doi.org/10.1007/s11581-016-1762-6

[5] Zhou Y, Zhang Y, Lin M, Long J, Zhang Z, Lin H, Wu J C S and Wang X 2015 *Nature Communications* **6** 8340 ISSN 2041-1723 URL https://doi.org/10.1038/ncomms9340

[6] Campos W E O, Nobre F X, da Rocha Filho G N, da Silva M A R, da Costa C E F, do Nascimento L A S and Zamian J R 2019 *Catalysts* **9** 667 ISSN 2073-4344 URL hhttps://doi.org/10.3390/catal9080667

[7] Zargazi M and Entezari M H 2019 *Applied Catalysis B: Environmental* **242** 507–517 ISSN 0926-3373 URL https://doi.org/10.1016/j.apcatb.2018.09.093

[8] Wang C, Ke X, Wang J, Liang R, Luo Z, Tian Y, Yi D, Zhang Q, Wang J, Han X F, Van Tendeloo G, Chen L Q, Nan C W, Ramesh R and Zhang J 2016 *Nature Communications* **7** 10636 ISSN 2041-1723 URL https://doi.org/10.1038/ncomms10636

[9] Zhou S, Liao L, Chen L, Feng B, He X, Bai X, Song C and Wu K 2023 *Nano Letters* **23** 7838–7844 ISSN 1530-6984 URL https://doi.org/10.1021/acs.nanolett.3c01426

[10] Kwon Y J, Yeo Y, Kim M S, Kim Y J, Park H S, Kim J, Choi S Y and Yang C H 2023 *Nano Letters* **23** 4557–4563 ISSN 1530-6984 URL https://doi.org/10.1021/acs.nanolett.3c01009

[11] Picozzi S 2014 *Frontiers in Physics* **2** 10 ISSN 2296-424X URL https://doi.org/10.3389/fphy.2014.00010

[12] Djani H, Garcia-Castro A C, Tong W Y, Barone P, Bousquet E, Picozzi S and Ghosez P 2019 *npj Quantum Materials* **4** 51 ISSN 2397-4648 URL https://doi.org/10.1038/s41535-019-0190-z

[13] Jeong J, Mun J, Das S, Kim J, Kim J R, Peng W, Kim M and Noh T W 2021 *ACS Applied Electronic Materials* **3** 1023–1030 ISSN 2637-6113 URL https://doi.org/10.1021/acsaelm.1c00005

[14] Mazzola F, Hassani H, Amoroso D, Chaluvadi S K, Fujii J, Polewczyk V, Rajak P, Koegler M, Ciancio R, Partoens B, Rossi G, Vobornik I, Ghosez P and Orgiani P 2023 *Journal of Physical Chemistry Letters* **14** 7208–7214 ISSN 1948-7185 URL https://doi.org/10.1021/acs.jpclett.3c01546

[15] Hwang J, Feng Z, Charles N, Wang X R, Lee D, Stoerzinger K A, Muy S, Rao R R, Lee D, Jacobs R, Morgan D and Shao-Horn Y 2019 *Materials Today* **31** 100–118 ISSN 13697021 URL https://doi.org/10.1016/j.mattod.2019.03.014

[16] Chen P, Du T, Jia H, Zhou L, Yue Q, Wang H and Wang Y 2022 *Applied Surface Science* **585** 152665 ISSN 0169-4332 URL https://doi.org/10.1016/j.apsusc.2022.152665

[17] Klein A, Albe K, Bein N, Clemens O, Creutz K A, Erhart P, Frericks M, Ghorbani E, Hofmann J P, Huang B, Kaiser B, Kolb U, Koruza J, Kübel C, Lohaus K N S, Rödel J, Rohrer J, Rheinheimer W, De Souza R A, Streibel V, Weidenkaff A, Widenmeyer M, Xu B X and Zhang H 2023 *Journal of Electroceramics* **51** 147–177 ISSN 1385-3449 URL https://doi.org/10.1007/s10832-023-00324-y

[18] Li T, Deng S, Liu H and Chen J 2024 *Chemical Reviews* **124** 7045–7105 ISSN 0009-2665 URL https://pubs.acs.org/doi/10.1021/acs.chemrev.3c00767

[19] Noguchi Y, Murata K and Miyayama M 2006 *Applied Physics Letters* **89** 242916 ISSN 0003-6951 URL https://doi.org/10.1063/1.2405408

[20] Das S, Ohkubo T, Kasai S and Kozuka Y 2021 *Crystal Growth & Design* **21** 625–630 ISSN 1528-7483 URL https://doi.org/10.1021/acs.cgd.0c01428

[21] Chaluvadi S K, Mondal D, Bigi C, Knez D, Rajak P, Ciancio R, Fujii J, Panaccione G, Vobornik I, Rossi G and Orgiani P 2021 *Journal of Physics: Materials* **4** 032001 ISSN 2515-7639 URL https://doi.org/10.1088/2515-7639/abe661

[22] Chaluvadi S K, Punathum Chalil S, Mazzola F, Dolabella S, Rajak P, Ferrara M, Ciancio R, Fujii J, Panaccione G, Rossi G and Orgiani P 2023 *Scientific Reports* **13** 3882 ISSN 2045-2322 URL https://doi.org/10.1038/s41598-023-30887-3

[23] Okudera H, Sakai Y, Yamagata K and Takeda H 2018 *Acta Crystallographica Section B Structural Science, Crystal Engineering and Materials* **74** 295–303 ISSN 2052-5206 URL https://doi.org/10.1107/SS2052520618006133

[24] Yoneda Y, Kohara S, Takeda H and Tsurumi T 2012 *Japanese Journal of Applied Physics* **51** 09LE06 ISSN 0021-4922 URL https://doi.org/10.1143/JJAP.51.09LE06

[25] Schlom D G, Chen L Q, Pan X, Schmehl A and Zurbuchen M A 2008 *Journal of the American Ceramic Society* **91** 2429–2454 ISSN 0002-7820 URL https://doi.org/0.1111/j.1551-2916.2008.02556.x

[26] Orgiani P, Chaluvadi S K, Chalil S P, Mazzola F, Jana A, Dolabella S, Rajak P, Ferrara M, Benedetti D, Fondacaro A, Salvador F, Ciancio R, Fujii J, Panaccione G, Vobornik I and Rossi G 2023 *Review of Scientific Instruments* **94** 033903 ISSN 0034-6748 URL https://doi.org/10.1063/5.0138889

[27] Troglia A, Bigi C, Vobornik I, Fujii J, Knez D, Ciancio R, Dražić G, Fuchs M, Sante D D, Sangiovanni G, Rossi G, Orgiani P and Panaccione G 2022 *Advanced Science* **9** 2105114 ISSN 2198-3844 URL https://doi.org/10.1002/advs.202105114

[28] Harrington G F and Santiso J 2021 *Journal of Electroceramics* **47** 141–163 ISSN 1385-3449 URL https://doi.org/10.1007/s10832-021-00263-6

[29] Bussolotti F, Lozzi L, Passacantando M, La Rosa S, Santucci S and Ottaviano L 2003 *Surface Science* **538** 113–123 ISSN 00396028 URL https://doi.org/10.1016/S0039-6028(03)00696-4

[30] Plumb N C, Salluzzo M, Razzoli E, Månsson M, Falub M, Krempasky J, Matt C E, Chang J, Schulte M, Braun J, Ebert H, Minár J, Delley B, Zhou K J, Schmitt T, Shi M, Mesot J, Patthey L and Radović M 2014 *Physical Review Letters* **113** 086801 ISSN 0031-9007 URL https://doi.org/10.1103/PhysRevLett.113.086801

[31] Gabel J, Zapf M, Scheiderer P, Schütz P, Dudy L, Stübinger M, Schlueter C, Lee T L, Sing M and Claessen R 2017 *Physical Review B* **95** 195109 ISSN 2469-9950 URL https://doi.org/10.1103/PhysRevB.95.195109

[32] Bigi C, Tang Z, Pierantozzi G M, Orgiani P, Das P K, Fujii J, Vobornik I, Pincelli T, Troglia A, Lee T L, Ciancio R, Drazic G, Verdini A, Regoutz A, King P D C, Biswas D, Rossi G, Panaccione G and Selloni A 2020 *Physical Review Materials* **4** 025801 ISSN 2475-9953 URL https://doi.org/10.1103/PhysRevMaterials.4.025801

[33] Yan X, Wrobel F, Tung I, Zhou H, Hong H, Rodolakis F, Bhattacharya A, McChesney J L and Fong D D 2022 *Advanced Materials* **34** ISSN 0935-9648 URL https://doi.org/10.1002/adma.202200866

[34] Toupet H, Le Marrec F, Holc J, Kosec M, Vilarhino P and Karkut M 2009 *Journal of Magnetism and Magnetic Materials* **321** 1702–1705 ISSN 0304-8853 URL https://doi.org/10.1016/j.jmmm.2009.02.024

[35] Orgiani P, Petrov A Y, Ciancio R, Galdi A, Maritato L and Davidson B A 2012 *Applied Physics Letters* **100** 042404 ISSN 0003-6951 URL https://doi.org/10.1063/1.3676268

[36] Knez D, Dražić G, Chaluvadi S K, Orgiani P, Fabris S, Panaccione G, Rossi G and Ciancio R 2020 *Nano Letters* **20** 6444–6451 ISSN 1530-6984 URL https://doi.org/10.1021/acs.nanolett.0c02125

[37] Di Pietro P, Bigi C, Chaluvadi S K, Knez D, Rajak P, Ciancio R, Fujii J, Mercuri F, Lupi S, Rossi G, Borgatti F, Perucchi A and Orgiani P 2022 *Advanced Electronic Materials* **8** 2101338 ISSN 2199-160X URL https://doi.org/10.1002/aelm.202101338

[38] Krishna D N G and Philip J 2022 *Applied Surface Science Advances* **12** 100332 ISSN 26665239 URL https://doi.org/10.1016/j.apsadv.2022.100332

[39] Takahashi R, Yamamoto T and Lippmaa M 2021 *Crystal Growth & Design* **21** 5017–5026 ISSN 1528-7483 URL https://doi.org/10.1021/acs.cgd.1c00456

[40] Suzuki S, Dazai T, Tokunaga T, Yamamoto T, Katoh R, Lippmaa M and Takahashi R 2024 *Journal of Applied Physics* **135** 195302 ISSN 0021-8979 URL https://doi.org/10.1063/5.0196987

[41] Lin Y C, Liu C, Yu Y, Zarkadoula E, Yoon M, Puretzky A A, Liang L, Kong X, Gu Y, Strasser A, Meyer H M, Lorenz M, Chisholm M F, Ivanov I N, Rouleau C M, Duscher G, Xiao K and Geohegan D B 2020 *ACS Nano* **14** 3896–3906 ISSN 1936-0851 URL https://doi.org/10.1021/acsnano.9b10196

[42] Panaccione G, Vobornik I, Fujii J, Krizmancic D, Annese E, Giovanelli L, Maccherozzi F, Salvador F, De Luisa A, Benedetti D, Gruden A, Bertoch P, Polack F, Cocco D, Sostero G, Diviacco B, Hochstrasser M, Maier U, Pescia D, Back C H, Greber T, Osterwalder J, Galaktionov M, Sancrotti M and Rossi G 2009 *Review of Scientific Instruments* **80** 043105 ISSN 0034-6748 URL https://doi.org/10.1063/1.3119364